PHARMACIA

Pharmacia 71: 1–9
DOI 10.3897/pharmacia.71.e122127

Research Article

Design, synthesis and biological evaluation of novel 2-hydroxy-1*H*-indene-1,3(2*H*)-dione derivatives as FGFR1 inhibitors

Mohammed M. Al-Mahadeen[1], Areej M. Jaber[2], Belal O. Al-Najjar[2,3]

1 *Chemistry Department, Faculty of Science, The University of Jordan, Amman, 11942, Jordan*
2 *Pharmacological and Diagnostic Research Center, Faculty of Pharmacy, Al-Ahliyya Amman University, Amman 19328, Jordan*
3 *Department of Pharmaceutical Sciences, Faculty of Pharmacy, Al-Ahliyya Amman University, 19328 Amman, Jordan*

Corresponding authors: Mohammed M. Al-Mahadeen (malmahadeen@yahoo.com); Areej M. Jaber (a.jaber@ammanu.edu.jo)

Received 2 March 2024 ♦ **Accepted** 31 March 2024 ♦ **Published** 23 April 2024

Citation: Al-Mahadeen MM, Jaber AM, Al-Najjar BO (2024) Design, synthesis and biological evaluation of novel 2-hydroxy-1*H*-indene-1,3(2*H*)-dione derivatives as FGFR1 inhibitors. Pharmacia 71: 1–9. https://doi.org/10.3897/pharmacia.71.e122127

Abstract

Fibroblast growth-factor receptor (FGFR) is a potential target for cancer therapy. We synthesised a novel series of FGFR1 inhibitors bearing quinoline, quinoxalin and isoquinoline using a synthetic strategy employing a one pot reaction, yielding 2-hydroxy-1*H*-indene-1,3(2*H*)-dione. Structural elucidation via IR, NMR and HRMS analyses is complemented by a proposed mechanistic pathway. All newly-synthesised compounds were evaluated in vitro for their inhibitory activities against FGFR-1. The most potent derivatives were 9a, 9b, 9c and 7b with IC_{50} = 5.7, 3.3, 4.1 and 3.1 μM, respectively, supported by molecular docking studies which probed the binding interactions of these compounds within the active site of the kinase.

Keywords

anticancer, Imidazo, Indene, FGFR1 inhibitor, molecular docking

To the memory of the late Prof. Mustafa M. El-Abadelah

Introduction

Aza-arenes (e.g. pyridine, quinoline, isoquinoline) are hyperaromatic aza-arene systems in which the bridgehead N-4 contributes to the aromaticity with its lone pair. Therefore, this nitrogen atom is not nucleophilic and the attack occurs at N-2 position. This parent compound is known to undergo electrophilic substitution (S_E–Ar) with various electrophiles at C-1, but also at C-3 or both, depending on the reaction conditions used (Katritzky et al. 2008). Consequently, acetylation of imidazo *N*-heterocycles commonly occurs at either the C-1 (Bower and Ramage 1955; Jaber et al. 2020) or C-3 (Hlasta and Silbernagel 1998) position, while nitrosation (followed by re-arrangement) typically targets the C-1 position (Paudler and Kuder 1967). Mono-formylation predominantly takes place at C-1 (70%) with a lesser extent at C-3 (30%) (Fuentes and Paudler 1975). Conversely, lithiation and related methods for generating carbanions favour C-3 (Paudler et al. 1972; Fuentes and Paudler 1975). When C-1 is blocked, electrophilic substitution primarily occurs at C-3 (Anderson and Watt 1995; Katritzky et al. 2008). Recently, El-Abadelah et al. investigated the reaction between 3-(substituted) imidazo[1,5-*a*]pyridines (1) and ninhydrin (2). This reaction involves the nucleophilic addition of the central carbonyl carbon of ninhydrin to C-1 of imidazo[1,5-*a*]pyridines, yielding the respective products 3a–g (Scheme 1) (Sammor et al. 2018; El-Abadelah et al. 2020; Al-Mahadeen et al. 2022; Jaber et al. 2023b).

PENSOFT

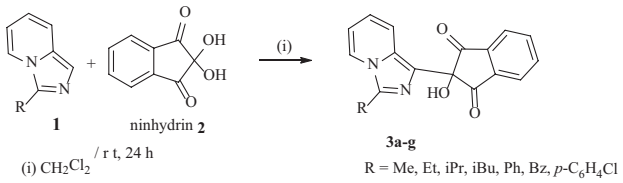

Scheme 1. Synthesis of 2-hydroxy-2-(imidazo[1,5-*a*]pyridinyl) indene-1,3(2*H*)-diones.

Depending on that, we deemed it valuable to examine the reaction between ninhydrin and imidazo N-heterocycles (such as quinoline, isoquinoline and quinoxaline) under neutral conditions. Additionally, we explored potential novel biological activities stemming from these reactions (,Shehadi et al. 2020; Jaber et al. 2022; Jaber et al. 2023a). Herein, we present our findings on both reactions, as depicted in Scheme 2 below, with a specific emphasis on their potential as inhibitors of fibroblast growth factor receptors (FGFR1).

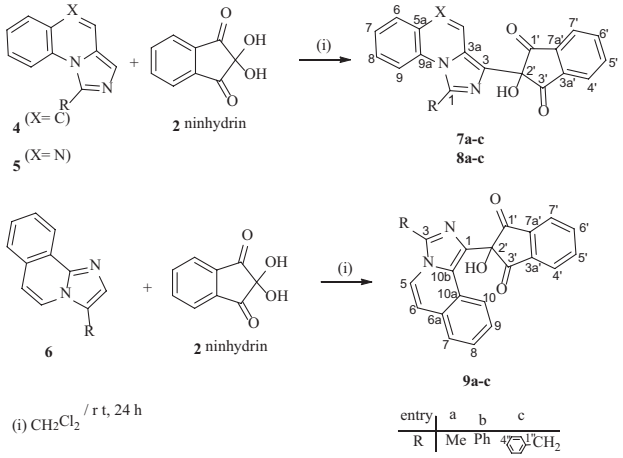

Scheme 2. Synthesis of compounds 7–9.

Materials and methods

Experimental part

Quinoline-2-carbaldehyde, isoquinoline-1-carbaldehyde, quinoxaline-2-carbaldehyde, dimethyl acetylenedicarboxylate (DMAD), ninhydrin, (±) Phenylglycine, L-phenylalanine, L-alanine and dichloromethane were procured from Acros. FTIR spectra were recorded using a Thermo-Nicolet Nexus 670 FTIR instrument. ^{1}H-NMR and ^{13}C-NMR spectra were acquired on a Bruker Avance III-500 MHz spectrometer with TMS serving as the internal standard. Chemical shifts were expressed as δ values in ppm. Carbon atom multiplicities were determined from DEPT experiments. High-resolution mass spectra (HRMS) were obtained using the electrospray ion trap (ESI) technique with collision-induced dissociation on a Bruker APEX-IV (7 Tesla) instrument. Solvents utilised in the study were sourced from Acros or Aldrich.

Chemistry

General procedure for the preparation of compounds (4–6)

These compounds were prepared from the reaction of appropriate amino acid with the appropriate aza-arene carboxaldehyde (in the presence of iodine I_2, potassium bicarbonate $KHCO_3$ and powder molecular sieves 4 Å) according to a reported procedure (Wang et al. 2012; Jaber et al. 2020; Al-Mahadeen et al. 2022).

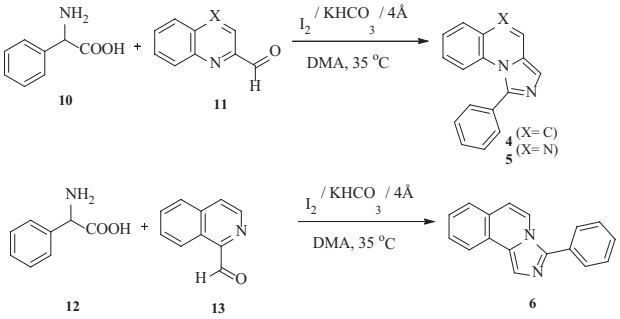

Scheme 3. Synthesis of compounds 4–6.

General procedure for synthesis compounds (7–9)

A solution containing 5 mmol of imidazo compounds 4–6 in 30 ml of anhydrous dichloromethane was added to a stirred solution of ninhydrin 2 (5 mmol) in 25 ml of dichloromethane at room temperature. The resulting mixture was stirred for an additional 3–4 hours at room temperature. Subsequently, the solvent was removed under vacuum, and the remaining crude product was purified by chromatographic separation on silica gel TLC plates, with elution achieved using a mixture of n-hexane and ethyl acetate (3:1, v/v).

2-hydroxy-2-(1-methylimidazo[1,5-a]quinolin-3-yl)-1H-indene-1,3(2H)-dione (7a)

Yield = 86%, yellowish solid, mp 205–207 °C; IR (KBR) = 3331, 3081, 1742, 1705, 1634, 1590, 1518, 1360, 1262, 1177, 1147, 1114, 1031 cm^{-1}; ^{1}H NMR (500 MHz, DMSO d_6) δ : 2.65 (s, 3H, 3-CH_3), 4.32 (br s, 1H, 2'-OH, exchangeable with D_2O), 7.05 (d, J = 9.0 Hz, 1H, H-5), 7.06 (ps t, 1H, H-8), 7.24 (ps t, 1H, H-7), 7.28 (d, J = 7.4 Hz, 1H, H-4), 7.53 (d, J = 8.0 Hz, 1H, H-6), 7.80 (ps t, 2H, H-5' / H-6'), 7.99, 8.01 (2d, J = 5.4 Hz, 2H, H-4' / H-7'); ^{13}C NMR (125 MHz, DMSO d_6) δ : 12.3 (3-CH_3), 78.2 (C-2'), 78.3 (C-2'), 117.4 (C-4), 117.5 (C-9), 122.9 (C-5), 124.2 (C-5' / C-6'), 125.5 (C-7), 125.6 (C-5a), 127.5 (C-8), 128.7 (C-6), 132.1 (C-3), 133.0 (C-9a), 136.3 (C-4' / C-7'), 141.0 (C-3'a / C-7'a), 141.1 (C-3'a / C-7'a), 141.4 (C-1), 197.2 (C-1' / C-3'), HRMS (ESI) *m/z* = Calcd: 343.09207 for $C_{21}H_{15}N_2O_3$, $[M+H]^+$, found: 343.09274.

2-hydroxy-2-(1-phenylimidazo[1,5-a]quinolin-3-yl)-1H-indene-1,3(2H)-dione (7b)

Yield = 61%, yellowish solid, m.p 110–112 °C; IR (KBR) = 3359, 2987, 2946, 1735, 1707, 1635, 1585, 1460, 1369,

1332, 1254, 1138, 1003 cm^{-1}; ^1H NMR (500 MHz, DMSO d_6) δ : 4.30 (s, 1H, 2'-OH, exchangeable with D_2O), 7.03 (d, *J* = 9.0 Hz, 1H, H-5), 7.07 (ps t, 1H, H-8), 7.24 (ps t, 1H, H-7), 7.28 (d, *J* = 7.4 Hz, 1H, H-4), 7.37 (ps t, 2H, H-3" / H-5"), 7.39 (ps t, 1H, H-4"), 7.43 (d, *J* = 6.8 Hz, 2H, H-2" / H-6"), 7.54 (d, *J* = 8.0 Hz, 1H, H-6), 7.78 (ps t, 2H, H-5' / H-6'), 7.97, 7.98 (2d, *J* = 5.4 Hz, 2H, H-4' / H-7'); ^{13}C NMR (125 MHz, DMSO d_6) δ : 78.3 (C-2'), 117.4 (C-4), 117.5 (C-9), 122.8 (C-5), 124.3 (C-5' / C-6'), 125.5 (C-7), 125.6 (C-5a), 127.5 (C-8), 128.7 (C-6), 128.9 (C-3" / C-5"), 129.2 (C-1"), 129.5 (C-4"), 129.8 (C-2" / C-6"), 132.1 (C-3), 133.0 (C-9a), 136.3 (C-4' / C-7'), 141.1 (C-3'a / C-7'a), 141.4 (C-1), 197.2 (C-1' / C-3'), HRMS (ESI) *m/z* = Calcd: 405.10772 for $C_{26}H_{17}N_2O_3$, $[M+H]^+$, found: 405.10810.

2-(1-benzylimidazo[1,5-a]quinolin-3-yl)-2-hydroxy-1H-indene-1,3(2H)-dione (7c)

Yield = 65%, yellowish solid, mp 180–182 °C; IR (KBR) = 3426, 3061, 1737, 1718, 1603, 1594, 1487, 1439, 1277, 1211, 1014 cm^{-1}; ^1H-^1H NMR (500 MHz, DMSO d_6) δ : 4.09 (br s, 1H, 2'-OH, exchangeable with D_2O), 4.12 (s, 2H, C*H*$_2$Ph), 7.03 (d, *J* = 9.0 Hz, 1H, H-5), 7.04 (d, *J* = 7.2 Hz, 2H, H-2" / H-6"), 7.19 (t, *J* = 7.0, 1H, H-4"), 7.22 (ps t, 2H, H-3" / H-5"), 7.07 (ps t, 1H, H-8), 7.24 (ps t, 1H, H-7), 7.28 (d, *J* = 7.4 Hz, 1H, H-4), 7.54 (d, *J* = 8.0 Hz, 1H, H-6), 7.78 (ps t, 2H, H-5' / H-6'), 7.97, 7.98 (2d, *J* = 5.4 Hz, 2H, H-4' / H-7'); ^{13}C NMR (125 MHz, DMSO d_6) δ : 33.2 (*C*H$_2$Ph), 78.4 (C-2'), 117.4 (C-4), 117.5 (C-9), 122.8 (C-5), 124.3 (C-5' / C-6'), 125.5 (C-7), 125.6 (C-5a), 126.8 (C-4"), 127.5 (C-8), 128.1 (C-2" / C-6"), 128.4 (C-6), 128.7 (C-3" /C-5"), 132.1 (C-3), 133.1 (C-9a), 135.7 (C-1"), 136.3 (C-4' / C-7'), 141.1 (C-3'a / C-7'a), 141.4 (C-1), 197.2 (C-1' / C-3'), HRMS (ESI) *m/z* = Calcd: 419.12337 for $C_{27}H_{19}N_2O_3$, $[M+H]^+$, found: 419.12325.

2-hydroxy-2-(1-methylimidazo[1,5-a]quinoxalin-3-yl)-1H-indene-1,3(2H)-dione (8a)

Yield = 66%), Yellowish solid, m.p 120–122 °C; IR (KBR) = 3028, 2711, 1754, 1737, 1718, 1603, 1594, 1487, 1439, 1277, 1211, 1014 cm^{-1}; ^1H NMR (500 MHz, DMSO d_6) δ : 2.70 (s, 3H, CH_3), 4.30 (s, 1H, 2'-OH, exchangeable with D_2O), 7.20 (t, *J* = 7.8 Hz, 1H, H-8), 7.42 (t, *J* = 7.8 Hz, 1H, H-7), 7.48 (d, *J* = 8.2 Hz, 1H, H-9), 7.94 (d, *J* = 7.9 Hz, 1H, H-6), 8.02 (ps t, 2H, H-5' / H-6'), 8.04 (ps t, 2H, H-4' / H-7'), 8.88 (s, 1H, H-4); ^{13}C NMR (125 MHz, DMSO d_6) δ : 79.3 (C-2'), 116.6 (C-9), 124.4 (C-5' / C-6'), 126.0 (C-9a), 126.7 (C-7), 127.7 (C-8), 130.3 (C-6), 132.0 (C-3), 136.0 (C-4' / C-7'), 137.2 (C-5a), 141.1 (C-3'a / C-7'a), 143.7 (C-1), 145.4 (C-4), 194.1 (C-1' / C-3'), HRMS (ESI) *m/z* = Calcd: 344.10172 for $C_{20}H_{14}N_3O_3$, $[M+H]^+$, found: 344.10110.

2-hydroxy-2-(1-phenylimidazo[1,5-a]quinoxalin-3-yl)-1H-indene-1,3(2H)-dione (8b)

Yield = 68%, yellowish solid, m.p 100–103 °C; IR (KBR) = 3028, 2711, 1754, 1714, 1593, 1551, 1419, 1367, 1320, 1259, 1174, 1146, 1107 cm^{-1}; ^1H NMR (500 MHz, DMSO d_6) δ : 4.30 (s, 1H, 2'-OH, exchangeable with D_2O), 7.20 (t, *J* = 7.8 Hz, 1H, H-8), 7.42 (t, *J* = 7.8 Hz, 1H, H-7), 7.48 (d, *J* = 8.2 Hz, 1H, H-9), 7.54 (ps t, 1H, H-4"), 7.55 (ps t, 2H, H-3" / H-5"), 7.65 (d, *J* = 8.4 Hz, 2H, H-2" / H-6"), 7.94 (d, *J* = 7.9 Hz, 1H, H-6), 8.02 (ps t, 2H, H-5' / H-6'), 8.04 (ps t, 2H, H-4' / H-7'), 8.88 (s, 1H, H-4); ^{13}C NMR (125 MHz, DMSO d_6) δ: 12.5 (3-CH_3), 79.3 (C-2'), 116.6 (C-9), 124.4 (C-5' / C-6'), 126.0 (C-9a), 126.7 (C-7), 127.7 (C-8), 129.0 (C-3" / C-5"), 129.7 (C-2" / C-6"), 130.1 (C-4"), 130.2 (C-6), 132.0 (C-3), 132.2 (C-1"), 136.0 (C-4' / C-7'), 137.2 (C-5a), 141.1 (C-3'a / C-7'a), 143.7 (C-1), 145.4 (C-4), 194.3 (C-1' / C-3'). HRMS (ESI *m/z* = Calcd: 406.10772 for $C_{25}H_{16}N_3O_3$, $[M+H]^+$, found: 406.10810.

2-(1-benzylimidazo[1,5-a]quinoxalin-3-yl)-2-hydroxy-1H-indene-1,3(2H)-dione (8c)

Yield = 65%, yellowish solid, mp 170–172 °C; IR (KBR) = 3308, 3020, 1737, 1702, 1603, 1517, 1477, 1439, 1233, 11471, 1014 cm^{-1}; ^1H-^1H NMR (500 MHz, DMSO d_6) δ : 4.35 (br s, 1H, 2'-OH, exchangeable with D_2O), 4.13 (s, 2H, C*H*$_2$Ph), 7.20 (t, *J* = 7.8 Hz, 1H, H-8), 7.42 (t, *J* = 7.8 Hz, 1H, H-7), 7.54 (ps t, 1H, H-4"), 7.55 (ps t, 2H, H-3" / H-5"), 7.65 (ps t, 2H, H-2" / H-6"), 7.94 (d, *J* = 7.9 Hz, 1H, H-6), 7.97 (ps t, 2H, H-5' / H-6'), 7.99 (2d, *J* = 5.4 Hz, 2H, H-4' / H-7'), 8.88 (s, 1H, H-4); ^{13}C NMR (125 MHz, DMSO d_6) δ : 33.4 (*C*H$_2$Ph), 79.3 (C-2'), 116.6 (C-9), 124.5 (C-5' / C-6'), 126.0 (C-9a), 126.7 (C-7), 127.7 (C-8), 129.0 (C-3" / C-5"), 129.7 (C-2" / C-6"), 130.1 (C-4"), 130.4 (C-6), 132.0 (C-3), 132.3 (C-1"), 136.0 (C-4' / C-7'), 137.2 (C-5a), 141.0 (C-3'a / C-7'a), 143.7 (C-1), 145.4 (C-4), 195.1 (C-1' / C-3'), HRMS (ESI *m/z* = Calcd: 420.10815 for $C_{26}H_{18}N_3O_3$, $[M+H]^+$, found: 420.10777.

2-hydroxy-2-(3-methylimidazo[5,1-a]isoquinolin-1-yl)-1H-indene-1,3(2H)-dione (9a)

Yield = 46%, yellowish solid, m.p 101–105 °C; IR (KBR) = 3331, 3081, 1742, 1705, 1634, 1590, 1518, 1360, 1262, 1177, 1147, 1114, 1031 cm^{-1}; ^1H NMR (500 MHz, DMSO d_6) δ : 2.65 (s, 3H, 3-C*H*$_3$), 4.32 (br s, 1H, 2'-OH, exchangeable with D_2O), 7.04 (d, *J* = 7.5 Hz, 1H, H-6), 7.47 (d, *J* = 7.5 Hz, 1H, H-7), 7.63 (t, *J* = 7.5 Hz, 1H, H-8), 7.71 (d, *J* = 7.6 Hz, 1H, H-9), 7.96 (ps t, 2H, H-5' / H-6'), 7.99 (ps t, 2H, H-4' / H-7'), 8.04 (d, *J* = 7.7 Hz, 1H, H-5); ^{13}C NMR (125 MHz, DMSO d_6) δ : 12.5 (3-CH_3), 80.2 (C-2'), 115.4 (C-6), 121.3 (C-5), 124.0 (C-4' / C-7'), 124.5 (C-10a), 127.0 (C-9), 128.0 (C-8), 128.2 (C-3a), 128.9 (C-10), 129.3 (C-6a), 137.03 (C-5' / C-6'), 139.2 (C-3), 140.9 (C-3'a / C-7'a), 198.5 (C-1' / C-3'), HRMS (ESI) *m/z* = Calcd: 343.09207 for $C_{21}H_{15}N_2O_3$, $[M+H]^+$, found: 343.09174.

2-hydroxy-2-(3-phenylimidazo[5,1-a]isoquinolin-1-yl)-1H-indene-1,3(2H)-dione (9b)

Yield = 56%, yellowish solid, m.p 108–111 °C; IR (KBR) = 3303, 3239, 1747, 1714, 1588, 1386, 1183, 1150, 1063 cm^{-1}, ^1H NMR (500 MHz, DMSO d_6) δ : 4.30 (s, 1H, 2'-OH, exchangeable with D_2O), 7.04 (d, *J* = 7.5 Hz, 1H, H-6), 7.42 (ps t, 1H, H-4"), 7.47 (d, *J* = 7.5 Hz, 1H, H-7), 7.50 (d, *J*

= 8.4 Hz, 2H, H-2" / H-6"), 7.51 (ps t, 2H, H-3" / H-5"), 7.63 (t, *J* = 7.5 Hz, 1H, H-8), 7.71 (d, *J* = 7.6 Hz, 1H, H-9), 7.96 (ps t, 2H, H-5' / H-6'), 7.98 (ps t, 2H, H-4' / H-7'), 8.04 (d, *J* = 7.7 Hz, 1H, H-5). ^{13}C-NMR (125 MHz, DMSO d_6) δ : 80.2 (C-2'), 115.4 (C-6), 121.3 (C-5), 124.0 (C-4' / C-7'), 124.5 (C-10a), 127.1 (C-9), 128.0 (C-8), 128.1 (C-4"), 128.2 (C-3a), 128.3 (C-2" / C-6"), 128.9 (C-10), 129.4 (C-6a), 129.5 (C-3" / C-5"), 130.8 (C-1"), 137.03 (C-5' / C-6'), 139.0 (C-3), 140.9 (C-3'a / C-7'a), 198.5 (C-1' / C-3'); HRMS (ESI) *m/z* = Calcd: 405.10772 for $C_{26}H_{17}N_2O_3$, $[M+H]^+$, found: 405.10710.

2-(3-benzylimidazo[5,1-a]isoquinolin-1-yl)-2-hydroxy-1H-indene-1,3(2H)-dione (9c)

Yield = 58%, yellowish solid, m.p 130–133 °C; IR (KBR) 3426, 3061, 1737, 1718, 1603, 1594, 1487, 1439, 1277, 1211, 1014 cm^{-1}; ^{1}H NMR (500 MHz, DMSO d_6) δ : 4.09 (br s, 1H, 2'-OH, exchangeable with D_2O), 4.11 (s, 2H, C*H*$_2$Ph), 7.00 (d, *J* = 7.2 Hz, 2H, H-2" / H-6"), 7.04 (d, *J* = 7.5 Hz, 1H, H-6), 7.19 (t, *J* = 7.0, 1H, H-4"), 7.22 (ps t, 2H, H-3" / H-5"), 7.42 (d, *J* = 7.5 Hz, 1H, H-7), 7.63 (t, *J* = 7.5 Hz, 1H, H-8), 7.71 (d, *J* = 7.6 Hz, 1H, H-9), 7.96 (ps t, 2H, H-5' / H-6'), 7.98 (ps t, 2H, H-4' / H-7'), 8.04 (d, *J* = 7.7 Hz, 1H, H-5); ^{13}C NMR (125 MHz, DMSO d_6) δ : 33.3 (*C*H$_2$Ph), 78.3 (C-2'), 115.4 (C-6), 121.3 (C-5), 124.0 (C-4' / C-7'), 124.5 (C-10a), 126.6 (C-4"), 127.0 (C-9), 128.0 (C-8), 128.1 (C-4"), 128.2 (C-3a), 128.9 (C-2" / C-6"), 129.3 (C-10), 129.4 (C-3" /C-5"), 129.6 (C-6a), 135.7 (C-1"), 137.03 (C-5' / C-6'), 139.1 (C-3), 140.9 (C-3'a / C-7'a), 198.5 (C-1' / C-3'), HRMS (ESI) *m/z* = Calcd: 419.12337 for $C_{27}H_{19}N_2O_3$, $[M+H]^+$, found: 419.12300.

Docking study

In our research, we aimed to better understand the molecular processes that contribute to the anticancer properties of the compound we synthesised. We used molecular docking simulations, specifically AutoDock 4.2.6 (Morris et al. 2009; Jaber et al. 2023a), to clarify this mechanism, using erdafitinib as a reference point for comparison. The simulations were made possible by using the crystal structure of FGFR1 when it is in a complex with erdafitinib (PDB ID: 5EW8) (Patani et al. 2016).

To prepare the protein and its potential binding molecules (ligands) for computer simulations, we used AutoDockTools (version 1.5.7) software. First, we loaded the 3D structure of the protein into the software and added missing hydrogen atoms and assigned electrical charges to improve its accuracy. Each candidate molecule was then loaded individually and its own electrical charges were assigned, based on its unique chemical makeup. Finally, we defined a specific region within the protein structure where the binding might occur. This region was centred around the location of a known FGFR1 inhibitor (erdafitinib) that was already present in the original crystal structure. The size of this defined region was set to be 15 Å^3, with a spacing of 0.375 Å between each grid point within the region. Docking simulations were conducted on a computer running Fedora Linux OS. The system comprised a Core i7-13620h CPU, 16 GB RAM and an Nvidia GeForce RTX 3090 GPU.

The docking simulations were carried out with standard settings, utilising a Lamarckian genetic algorithm over 100 iterations (Morris et al. 1998). Analysis of the AutoDock log files revealed the lowest energy of binding (LEB) values for each ligand, identifying the conformer with the most favourable binding energy. The chosen conformers were subsequently exported and visualised using BIOVIA Discovery Studio Visualizer 16.1 (Dassault-Systèmes 2016). This allowed us to gain a deeper understanding of the binding interactions amongst the synthesised compounds, the reference compound erdafitinib and the FGFR1 protein.

Biological evaluation

In vitro bioassay against fibroblast growth factor receptors (FGFR1) inhibitors

Human recombinant FGFR1 was obtained from Life Technology (CA, USA). Bioassays were conducted following the protocol provided by the supplier, utilising the Invitrogen Z'-LYTE® Kinase Assay Kit-Tyr 04 peptide, with FGFR-1 and ATP concentrations set at 6.0 nM and 25.0 μM, respectively. Hit molecules were prepared as stock solutions at 10.0 mM in DMSO, then serially diluted in buffer solution to achieve final concentrations ranging from 0.01 μM to 100.0 μM. The concentration of DMSO in the final kinase reaction did not exceed 1% (10.0 μl). IC50 values for each hit were determined using non-linear regression analysis of log (concentration) versus inhibition percentage values employing Graph Pad Prism 7.04.

Crystal structure

Crystals of compound **9b** were obtained through slow evaporation of a dilute DMSO solution, resulting in the formation of monoclinic pale-yellowish crystals. A suitable single crystal was epoxy-mounted on a glass fibre, with approximate dimensions of 0.378 × 0.287 × 0.078 mm^{-3}. Data collection was performed at room temperature (100 °K) using an Oxford Xcalibur diffractometer. The acquired data were processed to generate Shelxformat hkl files using CrysAlis Pro software from Agilent Technologies Ltd., Yarnton, Oxfordshire, UK. Cell parameters were determined and refined utilising the same software (Pro 2011). A multiscan absorption correction was applied during data collection. The crystal structure was solved using Direct Methods and refined by full-matrix least-squares on F^2 employing all unique data (Sheldrick 2015a, b). Anisotropic refinement was performed for all non-hydrogen atoms, while hydrogen atoms were positioned using a riding model and refined isotropically. Isotropic displacement parameters for hydrogen atoms were set at 1.2 times those of the bonded carbon atoms. Crystallographic data summary is provided in Table 1. Supplementary crys-

tallographic data for this study can be accessed through CCDC 2333010 at The Cambridge Crystallographic Data Centre (www.ccdc.cam.ac.uk/data_request/cif).

Results and discussion

Chemistry

In this study, the direct interaction of ninhydrin 2 with the imidazo derivatives 4–6 in dichloromethane at room temperature yielded the expected adducts 7–9 in high yields Scheme 2. The newly-synthesised compounds underwent identification and characterisation using IR, NMR and HRMS spectral data and their structures were validated through single-crystal X-ray structure determination. The collected data consistently supported the proposed structures. Notably, mass spectra exhibited accurate molecular ion peaks and HRMS spectral data aligned closely with calculated values. DEPT and 2D (COSY, HMQC and HMBC) experiments aided in assigning signals to different carbons and their attached and neighbouring hydrogens. We confirmed the structures by single crystal X ray structure determination for 9b (Fig. 1), representing the series.

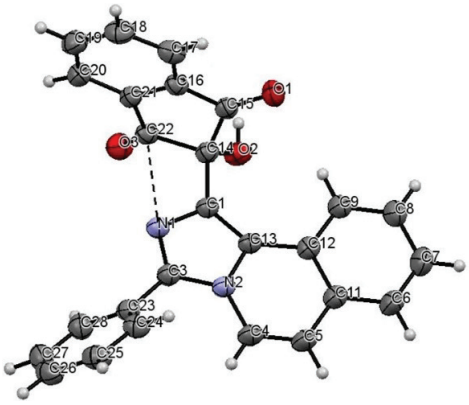

Figure 1. ORTEP view of the molecular structure and atom numbering scheme of 9b.

X-ray structure determination of 9b

To confirm the structure of 9b (Scheme 2), X-ray crystal structure determination was conducted. A summary of the data collection and refinement parameters is provided in Table 1. The molecular structure of 9b, as derived from crystallographic data, is depicted in Fig. 1. Notably, the two aromatic systems exhibit a nearly perpendicular orientation to each other, with an angle of 81° between their respective planes. This perpendicular alignment is stabilised by attractive forces between N1 and the carbonyl carbon (C22), with a distance of 2.744 Å between the two atoms, approximately 0.5 Å less than the sum of van der Waal's radii. Such interactions between electron-deficient carbon atoms of carbonyl groups and electronegative atoms have been frequently documented in the literature (Braga et al. 2009).

Table 1. Crystal data and structure refinement for 9b.

Empirical formula	$C_{28}H_{22}N_2O_4S$
Formula weight, g mol^{-1}	482.53
Temperature, K	100
Crystal system	monoclinic
Space group	$P2_1/n$
a, Å	16.525(6)
b, Å	8.346(3)
c, Å	17.532(7)
α/°	90
β/°	103.530(12)
γ/°	90
Volume, Å^3	2350.9(15)
Z	4
Density (calcd.), g cm^{-3}	1.363
Absorption coefficient μ/mm^{-1}	0.176
F (000), e	1008.0
2Θ range for data collection, deg	3.87 to 61.194
Index ranges *hkl*	$-21 \le h \le 23$, $-11 \le k \le 11$, $-25 \le l \le 24$
Reflections collected	83166
Independent reflections	7175 [R_{int} = 0.0884, R_{sigma} = 0.0421]
Absorption correction	Semi-empirical from equivalents
Refinement method	Full-matrix least-squares on F^2
Data/ restraints/ parameters	7175/ 0/ 320
Final R indexes [I ≥ 2σ (I)]	R_1 = 0.0547, wR_2 = 0.1391
Final R indexes [all data]	R_1 = 0.0775, wR_2 = 0.1681
Largest diff. peak/hole, e Å^{-3}	0.29/-0.42

[a]$R1 = \Sigma||Fo| - |Fc||/\Sigma|Fo|$; [b]$wR2 = [\Sigma w(F_o^2 - F_c^2)^2/\Sigma w(F_o^2)^2]^{1/2}$.

Molecular docking

Molecular docking simulations were performed to shed light on the molecular processes that contribute to the anticancer effects of the created compounds on the FGFR1 protein. To ensure the accuracy of the docking process, the co-crystal structure of erdafitinib was re-docked Fig. 2, resulting in an RMSD value of 0.76 Å, as shown in Fig. 3. The RMSD value, which is less than the 2 Å limit, verifies the dependability of the docking protocol for future analyses (Hevener et al. 2009).

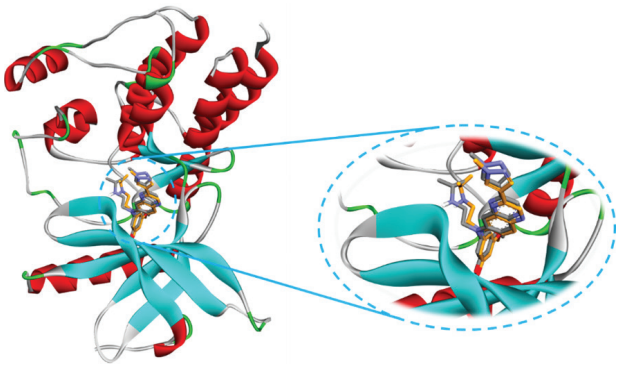

Figure 2. Solid ribbon representation of FGFR1 (PDB ID: 5EW8) with co-crystal (grey) and re-docked (orange) erdafitinib. Generated by Biovia Discovery Studio visualizer®.

The molecular docking simulation results for the compounds 7b, 9a, 9b and 9c against FGFR1 are presented in Table 2. The free energy of binding (in kcal/mol) indicates

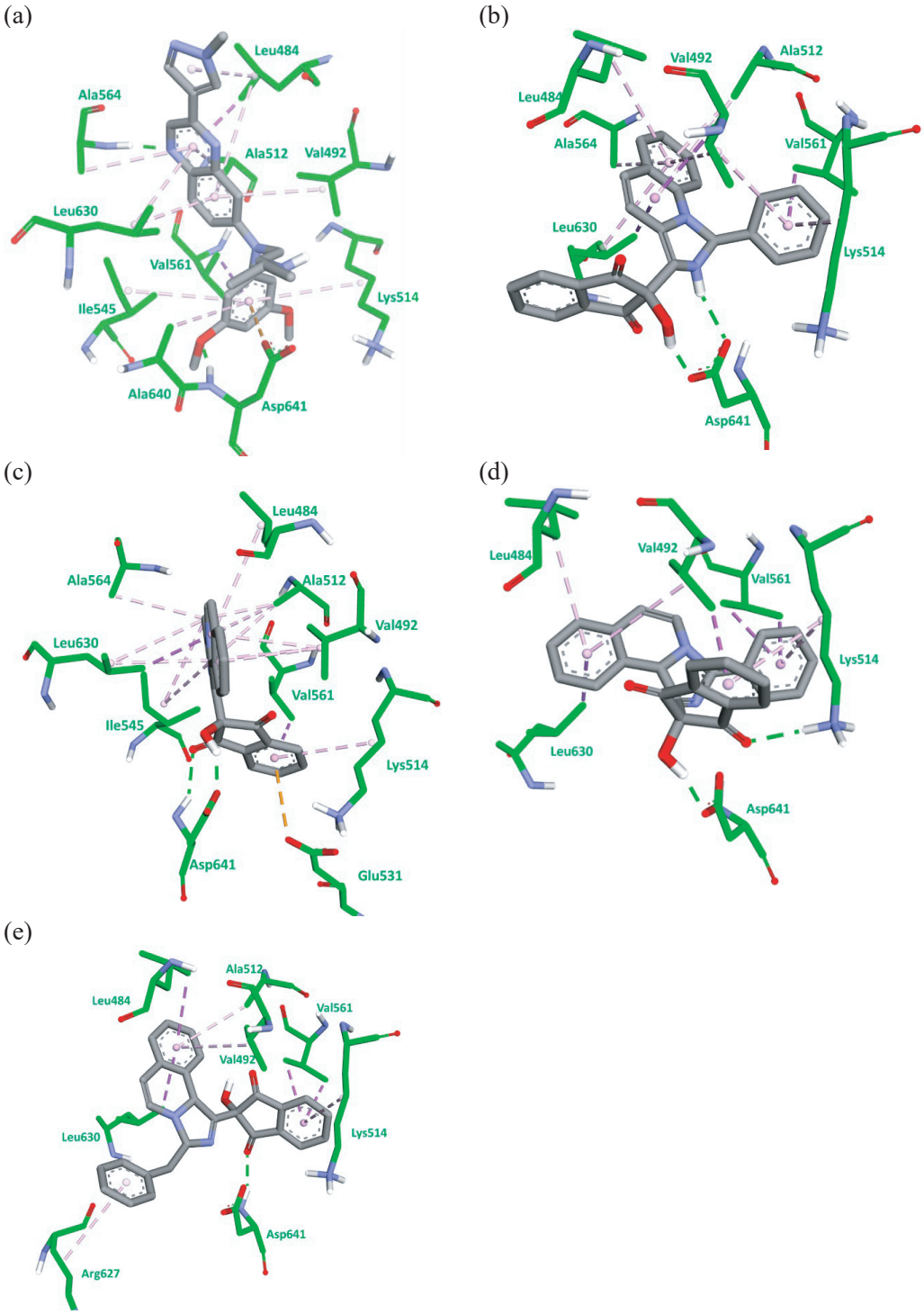

Figure 3. Stick representation of **a.** Erdafitinib; **b.** 7b; **c.** 9a; **d.** 9b; **e.** 9c in grey colour, docked within FGFR1 (PDB ID: 5EW8) binding site (green). Generated by Biovia Discovery Studio visualizer®.

Table 2. Lowest binding Energy in kcal/mol of the Docked Compounds 7b, 9a, 9b and 9c against FGFR1 binding site.

#	Compound	Lowest Binding Energy (kcal/mol)	Interacting Residues		
			Hydrogen Bond	Hydrophobic	Pi-Anion
1.	**7b**	**-8.97**	Asp641	Leu484, Val492, Ala512, Lys514, Val561, Ala564, Leu630	NI
2.	**9a**	**-8.02**	Asp641	Leu484, Val492, Ala512, Lys514, Ile545 Val561, Ala564, Leu630	Glu531
3.	**9b**	**-9.23**	Lys514, Asp641	Leu484, Val492, Lys514, Val561, Leu630	NI
4.	**9c**	**-9.18**	Asp641	Leu484, Val492, Ala512, Lys514, Val561, Arg627, Leu630	NI
5.	Erdafitinib (Reference)	**-11.16**	Ala564, Asp641	Leu484, Val492, Ala512, Lys514, Ile545, Val561, Leu630, Ala640	Asp641

NI = No Interaction.

the strength of the interaction between the compound and the target protein, with lower values indicating stronger interactions.

Compound 7b exhibits a free energy of binding of -8.97 kcal/mol, with Asp641 performing hydrogen bond interaction and several residues (Leu484, Val492, Ala512, Lys514, Val561, Ala564, Leu630) performing hydrophobic interactions. However, no Pi-Anion interactions were observed. Compound 9a shows a slightly weaker binding energy of -8.02 kcal/mol. It interacts with Asp641 through hydrogen bonding and with several residues (Leu484, Val492, Ala512, Lys514, Ile545, Val561, Ala564, Leu630) through hydrophobic interactions. Notably, it also exhibits Pi-Anion interactions with Glu531. Compounds 9b and 9c exhibit stronger binding energies of -9.23 kcal/mol and -9.18 kcal/mol, respectively. Compound 9b forms hydrogen bonds with Lys514 and Asp641 and hydrophobic interactions with Leu484, Val492, Lys514, Val561 and Leu630. Compound 9c forms a hydrogen bond with Asp641 and hydrophobic interactions with Leu484, Val492, Ala512, Lys514, Val561, Arg627 and Leu630. Neither compound shows Pi-Anion interactions. For comparison, the reference compound Erdafitinib exhibits a binding energy of 11.16 kcal/mol, indicating a stronger interaction with FGFR1. It forms hydrogen bonds with Ala564 and Asp641, hydrophobic interactions with Leu484, Val492, Ala512, Lys514, Ile545, Val561, Leu630 and Ala640 and a Pi-Anion interaction with Asp641.

An interesting trend emerged, suggesting a moderate correlation between the predicted binding affinity and the in vitro inhibitory activity. Compound 9b, which exhibited the most favourable docking score (Lowest Binding Energy = -9.23 kcal/mol) with additional hydrogen bond interaction with Lys514, Asp641, also displayed the most potent inhibitory effect (IC_{50} = 3.3 μM).

Similarly, compound 7b, with the second-highest binding affinity (-8.97 kcal/mol) and interaction with Asp641, demonstrated a notable inhibitory effect (IC_{50} = 3.1 μM).

However, a perfect correlation was not observed. Compounds 9c and 9a displayed comparable binding energies (-9.18 and -8.02 kcal/mol, respectively) and interacted with Asp641. However, their in-vitro potencies differed, with 9c exhibiting a lower IC_{50} (4.1 μM) compared to 9a (5.7 μM). This discrepancy suggests that other factors beyond the predicted binding energy and the primary interacting residues might also influence the inhibitory activity of these compounds.

Evaluation of biological activities

We assessed the cytotoxic activities of the prepared compounds against fibroblast growth factor receptors (FGFR1) inhibitors. Notably, Table 3 shows the inhibitory profiles of 7a-c, 8a-c and 9a-c. Clearly, 7b, 9a, 9b and 9c have superior inhibitory percentages compared to other compounds prompting us to pursue their IC_{50} values. Fig. 4 shows the resulting dose/response curves and IC_{50} values.

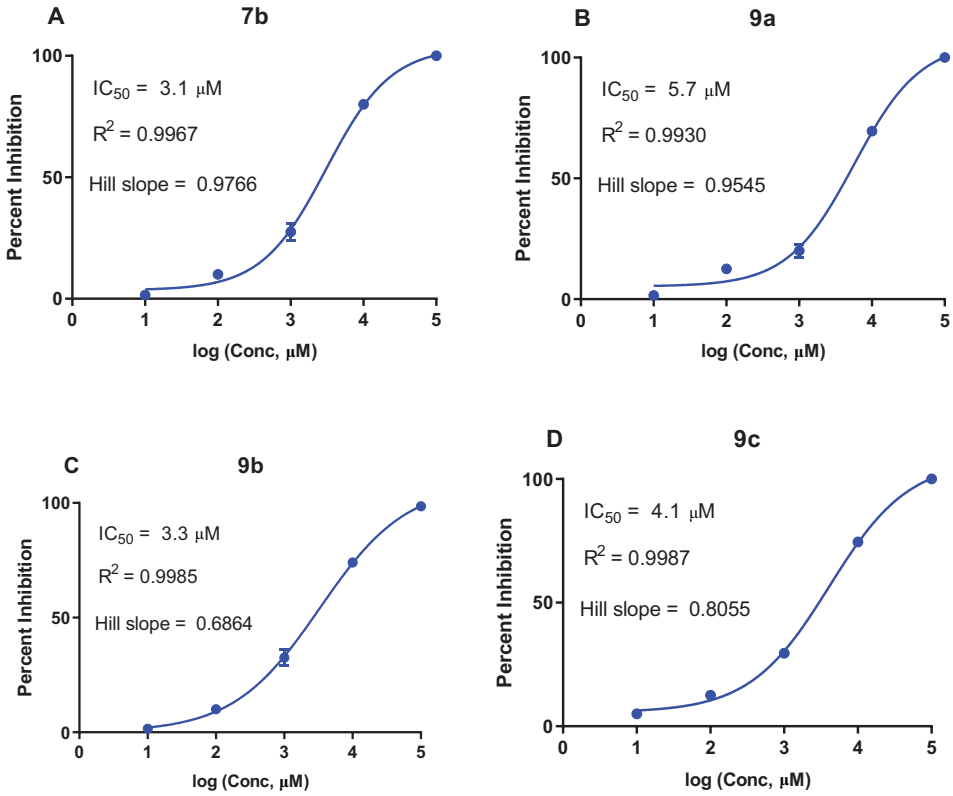

Figure 4. Dose-response curves of compounds 7b, 9a, 9b and 9c FGFR1 inhibitor. **A.** Dose-response curve of 7b with IC_{50} = 3.1 μM; **B.** Dose-response curve of 9a with IC_{50} = 5.7 μM; **C.** Dose-response curve of 9b with IC_{50} = 3.3 μM; **D.** Dose-response curve of 9c with IC_{50} = 4.1 μM.

Table 3. Percent inhibition values of FGFR1 at 10 μM concentration of the prepared compounds. Staurosporine was included as a control.

Compound	% Inhibition at 10 μM[a]	IC_{50} (μM)
7a	8	ND[b]
7b	40	3.1
7c	12	ND[b]
8a	6	ND[b]
8b	8	ND[b]
8c	7	ND[b]
9a	43	5.7
9b	32	3.3
9c	39	4.1
Staurosporine[c]	12.12 nM	

[a]Average of duplicate measurements ± standard deviation.
[b]ND: Not determined.
[c]Standard inhibitor.

Conclusions

This study explores a novel range of compounds featuring quinoline, quinoxalin and isoquinoline as potential inhibitors of FGFR1. These compounds were synthesised via the direct interaction of ninhydrin with imidazo derivatives. In vitro testing revealed that, while all compounds exhibited weak inhibitory activity against FGFR1, compounds 9a, 9b, 9c and 7b demonstrated IC_{50} values of 5.7, 3.3, 4.1 and 3.1 μM, respectively. Molecular docking simulations on the FGFR1 protein binding site suggested that the anticancer effects may arise from enzyme inhibition. Additionally, in silico studies indicated favourable pharmacokinetic properties, offering promise for the development of novel cancer therapeutics with enhanced efficacy and specificity in the future.

Acknowledgements

The authors would like to pay tribute to the late Professor Mustafa M. El-Abadelah, who was always willing to offer guidance and support throughout his professional and scientific career.

References

Al-Mahadeen MM, Zahra JA, El-Abadelah MM, Jaber AM, Khanfar MA (2022) One-pot synthesis of novel 2-oxo (2H)-spiro [benzofuran-3, 3'-pyrrolines] via 1, 4-dipolar cycloaddition reaction. Results in Chemistry 4: 100643. https://doi.org/10.1016/j.rechem.2022.100643

Anderson DJ, Watt W (1995) The reaction of imidazo [1, 5-a] pyridines with methyl-and phenyltriazolinediones and with diethyl azodicarboxylate. Journal of heterocyclic chemistry 32(5): 1525–1530. https://doi.org/10.1002/jhet.5570320520

Bower JD, Ramage GR (1955) Heterocyclic systems related to pyrrocoline. Part I. 2: 3a-Diazaindene. Journal of the Chemical Society [Resumed] 0: 2834–2837. https://doi.org/10.1039/jr9550002834

Braga D, Grepioni F, Maini L, Polito M (2009) Crystal polymorphism and multiple crystal forms. In: Hosseini M (Ed.) Molecular Networks. Structure and Bonding, Vol. 132. Springer, Berlin, Heidelberg, 87–95. https://doi.org/10.1007/978-3-642-01367-6_7

Dassault-Systèmes (2016) Biovia, discovery studio modeling environment (Version 16.1). https://www.3ds.com/

El-Abadelah MM, Awwadi FF, Abdullah AH, Voelter W (2020) The reaction of imidazo [1, 5-a] pyridines with ninhydrin revisited. Zeitschrift für Naturforschung B 75(6–7): 559–565. https://doi.org/10.1515/znb-2020-0027

Fuentes O, Paudler WW (1975) Some formylation reactions of imidazo [1, 5-a] pyridine and pyrrocoline. Journal of Heterocyclic Chemistry 12(2): 379–383. https://doi.org/10.1002/jhet.5570120235

Hevener KE, Zhao W, Ball DM, Babaoglu K, Qi J, White SW, Lee RE (2009) Validation of molecular docking programs for virtual screening against dihydropteroate synthase. Journal of Chemical Information and Modeling 49(2): 444–460. https://doi.org/10.1021/ci800293n

Hlasta DJ, Silbernagel MJ (1998) The regioselective acylation reactions of imidazopyridines. Heterocycles 5(48): 1015–1022. https://doi.org/10.3987/COM-98-8124

Jaber AM, Zahra JA, El-Abadelah MM, Sabri SS, Khanfar MA, Voelter W (2020) Utilization of 1-phenylimidazo [1, 5-a] quinoline as partner in 1, 4-dipolar cycloaddition reactions. Zeitschrift für Naturforschung B 75(3): 259–267. https://doi.org/10.1515/znb-2019-0150

Jaber AM, Zahra JA, Sabri SS, Khanfar MA, Awwadi FF, El-Abadelah MM (2022) New Trends in 1, 4-Dipolar Cycloaddition Reactions. Thermodynamic Control Synthesis of Model 2'-(isoquinolin-1-yl)-spiro [oxindole-3, 3'-pyrrolines]. Current Organic Chemistry 26(5): 542–549. https://doi.org/10.1515/znc-2022-0085

Jaber AM, Al-Mahadeen MM, Al-Qawasmeh RA, Taha M (2023a) Synthesis, anticancer evaluation and docking studies of novel adamantanyl-1, 3, 4-oxadiazol hybrid compounds as Aurora-A kinase inhibitors. Medicinal Chemistry Research, 11 pp. https://doi.org/10.21203/rs.3.rs-3161447/v1

Jaber AM, Zahra JA, El-Abadelah MM, Sabri SS, Sabbah DaS (2023b) Thermodynamic control synthesis of spiro [oxindole-3, 3'-pyrrolines] via 1, 4-dipolar cycloaddition utilizing imidazo [1, 5-a] quinoline. Zeitschrift für Naturforschung C 78(3–4): 141–148. https://doi.org/10.1515/znc-2022-0085

Katritzky AR, Ramsden CA, Scriven EF, Taylor RJ, Jones RC (2008) Comprehensive heterocyclic chemistry iii.: Ring systems with at least two fused heterocyclic five-or six-membered rings with no bridgehead heteroatom. Elsevier Limited.

Morris GM, Goodsell DS, Halliday RS, Huey R, Hart WE, Belew RK, Olson AJ (1998) Automated docking using a Lamarckian genetic algorithm and an empirical binding free energy function. Journal of Computational Chemistry 19(14): 1639–1662. https://doi.org/10.1002/(SICI)1096-987X(19981115)19:14%3C1639::AID-JCC10%3E3.0.CO;2-B

Morris GM, Huey R, Lindstrom W, Sanner MF, Belew RK, Goodsell DS, Olson AJ (2009) AutoDock4 and AutoDockTools4: Automated docking with selective receptor flexibility. J Comput Chem 30(16): 2785–2791. https://doi.org/10.1002/jcc.21256

Patani H, Bunney TD, Thiyagarajan N, Norman RA, Ogg D, Breed J, Ashford P, Potterton A, Edwards M, Williams SV, Thomson GS,

Pang CSM, Knowles MA, Breeze AL, Orengo C, Phillips C, Katan M (2016) Landscape of activating cancer mutations in FGFR kinases and their differential responses to inhibitors in clinical use. Oncotarget 7(17): 24252–24268. https://doi.org/10.18632/oncotarget.8132

Paudler WW, Kuder JE (1967) The conversion of imidazo [1, 5-a] pyridines into 3-(2-pyridyl)-1, 2, 4-oxadiazoles. The Journal of Organic Chemistry 32(8): 2430–2433. https://doi.org/10.1021/jo01283a015

Paudler WW, Patsy Chao C, Ilelmick LS (1972) Phenyllithium addition reactions of some polyazaindenes. Journal of Heterocyclic Chemistry 9(5): 1157–1160. https://doi.org/10.1002/jhet.5570090539

Pro C (2011) Software System (version 1.171.35.11), Intelligent Data Collection and Processing Software for Small Molecule and Protein Crystallography. Yarnton, Oxfordshire (UK), Agilent Technologies Ltd.

Sammor MS, El-Abadelah MM, Hussein AQ, Awwadi FF, Sabri SS, Voelter W (2018) A study on the reaction of 3-alkyl (aryl) imidazo [1, 5-a] pyridines with ninhydrin. Zeitschrift für Naturforschung B 73(6): 413–421. https://doi.org/10.1515/znb-2018-0039

Shehadi IA, Delmani F-A, Jaber AM, Hammad H, AlDamen MA, Al-Qawasmeh, RA Khanfar M AJM (2020) Synthesis, characterization and biological evaluation of metal adamantyl 2-pyridylhydrazone complexes. Molecules 25(11): 2530. https://doi.org/10.3390/molecules25112530

Sheldrick GM (2015a) Crystal structure refinement with SHELXL. Acta Crystallographica Section C: Structural Chemistry 71(1): 3–8. https://doi.org/10.1107/S2053229614024218

Sheldrick GM (2015b) SHELXT–Integrated space-group and crystal-structure determination. Acta Crystallographica Section A: Foundations Advances 71(1): 3–8. https://doi.org/10.1107/S2053273314026370

Wang Q, Zhang S, Guo F, Zhang B, Hu P, Wang (2012) Natural α-amino acids applied in the synthesis of imidazo [1, 5-a] N-heterocycles under mild conditions. The Journal of Organic Chemistry 77(24): 11161–11166. https://doi.org/10.1021/jo302299u

Supplementary material 1

Design, synthesis and biological evaluation of novel 2-hydroxy-1H-indene-1,3(2H)-dione derivatives as FGFR1 inhibitors

Authors: Mohammed M. Al-Mahadeen, Areej M. Jaber, Belal O. Al-Najjar

Data type: pdf

Link: https://doi.org/10.3897/pharmacia.71.e122127.suppl1